Appl Phys A (2013) 110:93–98
DOI 10.1007/s00339-012-7417-1

Applied Physics A
Materials Science & Processing

Reducing the thermal conductivity of silicon by nanostructure patterning

Y.W. Wen · H.J. Liu · L. Pan · X.J. Tan · H.Y. Lv · J. Shi · X.F. Tang

Received: 18 April 2012 / Accepted: 29 October 2012 / Published online: 15 November 2012

Abstract Based on molecular dynamics simulations, we propose using nanostructure-patterned silicon for thermoelectric applications. Three typical examples are (i) fractal-like nanoporous Si, (ii) etched Si nanofilm, and (iii) quasi-periodic layered SiGe. All of them can exhibit very low thermal conductivity (less than 1.0 $\mathrm{W\,m^{-1}\,K^{-1}}$) and may be mass produced with standard fabrication techniques such as molecular beam epitaxy or Czochralski process. By maintaining good electronic transport of bulk Si, it is possible to achieve $ZT \sim 5.0$ at room temperature.

1 Introduction

There are tremendous on-going efforts in searching for new thermoelectric materials with high enough efficiency, which can be quantified by the well-known figure of merit:

$$ZT = \frac{S^2 \sigma T}{\kappa_e + \kappa_l}. \tag{1}$$

Here S is the Seebeck coefficient, σ is the electric conductivity, T is the absolute temperature. κ_e and κ_l are the electronic and lattice thermal conductivity, respectively. A higher ZT value indicates good thermoelectric performance, and one therefore must try to maximize the power factor ($S^2\sigma$) and/or minimize the thermal conductivity ($\kappa = \kappa_e + \kappa_l$). However, these transport coefficients (S, σ, and κ) are coupled to each other and related to the carrier concentrations and crystal structures, it becomes very difficult to optimize all of them at the same time. As a result, most thermoelectric materials exhibit a ZT value less than 1.0, which cannot compete with conventional refrigerators or power generators. It was shown [1, 2], that much higher ZT value can be achieved in low-dimensional systems or nanostructures. However, the practical implementation of them remains a fundamental barrier so far.

As the most abundant and widely used semiconductor, Si has attracted growing attention for its promising thermoelectric applications. Bulk Si, however, is a poor thermoelectric material because of its high thermal conductivity (∼150 $\mathrm{W\,m^{-1}\,K^{-1}}$), giving a $ZT \sim 0.01$ at room temperature. It is reported that alloying with Ge to form SiGe nanocomposites [3–6] or superlattice [7–10], could suppress the thermal conductivity to 2∼10 $\mathrm{W\,m^{-1}\,K^{-1}}$. However, the obtained ZT value is still too low to be competitive. Another efficient way is using low dimensional Si structures, such as nanowires (NWs), which can reduce the thermal conductivity by two orders of magnitude due to surface scattering of phonons [11–13]. Moreover, it was theoretically shown that the thermal conductivity of Si NWs is diameter-dependent and can be further reduced by surface roughness [14–17]. The SiGe NWs, on the other hand, were found to exhibit a very low thermal conductivity less than 1.0 $\mathrm{W\,m^{-1}\,K^{-1}}$ [18]. Nevertheless, the mass production of certain Si or SiGe NWs and implementing them into a device are not easy,

Y.W. Wen · H.J. Liu (✉) · L. Pan · X.J. Tan · H.Y. Lv · J. Shi
Key Laboratory of Artificial Micro- and Nano-structures of Ministry of Education and School of Physics and Technology, Wuhan University, Wuhan 430072, China
e-mail: phlhj@whu.edu.cn

Y.W. Wen
Department of Materials Science and Engineering, Huazhong University of Science and Technology, Wuhan 430074, Hubei, China

X.F. Tang
State Key Laboratory of Advanced Technology for Materials Synthesis and Processing, Wuhan University of Technology, Wuhan 430070, China

which may limit their thermoelectric applications. Recent work found that nanoporous Si (*np*Si) has a very low thermal conductivity across the pores [19–22] and can maintain good electronic transport properties of bulk Si, thus the *ZT* value can be enhanced by two orders of magnitude [23]. Unfortunately, to decrease the thermal conductivity below 1.0 $\mathrm{W\,m^{-1}\,K^{-1}}$, the pores must be very closely-packed and have size as small as 0.6 nm, which is very difficult to produce in a real process. In this work, we show that by nanostructure patterning, the thermal conductivity of silicon can be reduced to less than 1.0 $\mathrm{W\,m^{-1}\,K^{-1}}$. Three typical examples we would like to show are (i) fractal-like nanoporous Si (*np*Si), (ii) etched Si nanofilm, and (iii) quasi-periodic layered SiGe. All of them can be easily accessible from a manufacturing point of view, and may have very promising thermoelectric applications.

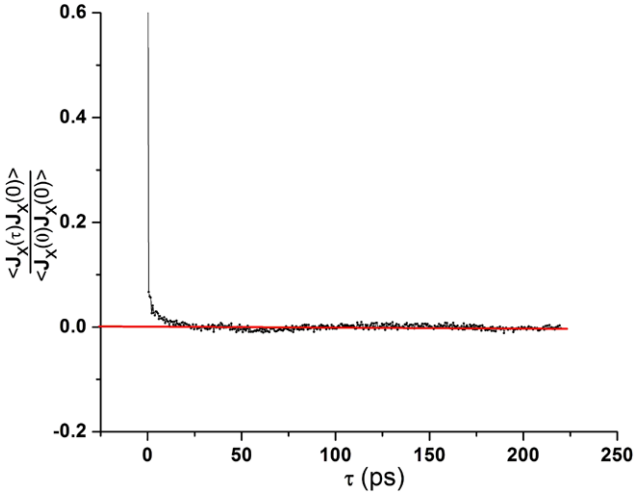

Fig. 1 Normalized heat current autocorrelation function of 3.2 nm *np*Si as a function of MD time

2 Computational method

Our calculations are performed by using the molecular dynamics (MD) as implemented in the LAMMPS code [24]. The thermal conductivity is calculated from heat current autocorrelation function according to the Green–Kubo relation:

$$\kappa_{\mu v}(\tau_m) = \frac{1}{\Omega k_B T^2} \int_0^{\tau_m} \left\langle J_\mu(\tau) J_v(0) \right\rangle d\tau \tag{2}$$

where Ω is the system volume, k_B is the Boltzmann constant, T is the system temperature, $J_\mu(\tau)$ is the μth component of the heat flux, and the angular brackets indicate an ensemble average (or an average over time in the case of MD simulations). Such a method is usually referred to as equilibrium molecular dynamics (EMD) and was initially used by Hoover et al. [25, 26] to compare transport coefficients of flow system calculated from non-equilibrium molecular dynamics (NEMD). In the subsequent works, Evans and Ciccotti et al. [27–31] performed both EMD and NEMD using either an approximate or rigorous expression for the microscopic heat flux, and found consistent values for the transport coefficients. In the present work, the integration in Eq. (2) is replaced by summation, and what we actually compute is [32]:

$$\kappa_{\mu v}(\tau_M) = \frac{\Delta t}{\Omega k_B T^2} \sum_{m=1}^{M} (N-m)^{-1} \sum_{n=1}^{N-m} J_\mu(m+n) J_v(n) \tag{3}$$

where N denotes the total number of MD steps, M is the number of steps for integration, Δt is the time step which is set to 0.55 fs in our simulations, and τ_M is given by $M\Delta t$. For accurate statistical averaging, a very large N should be used and appropriate M must be chosen to decay the heat current autocorrelation function to zero. We use a Stillinger–Weber [33] potential for the pure Si systems and Tersoff [34] potential for the SiGe systems. These potentials include both two- and three-body interactions and can accurately predict the thermal properties of Si and Ge systems. In fact, they have been successful in calculating the thermal conductivity of Si and Ge nanostructures [12, 17, 18, 23, 35]. To ensure that the system has reached an equilibrium state, a constant temperature simulation of 400,000 steps and a constant energy simulation of 200,000 steps are carried out. After that, a total of 8,000,000 MD steps (4.4 ns) are performed to record the heat current and 400,000 steps are selected (220 ps) to calculate the thermal conductivity according to Eq. (3). This turns out to be a reliable setting as indicated in Fig. 1 where the normalized heat current autocorrelation function for an *np*Si with pore size of 3.2 nm decays to zero after 150 ps MD time. Since we are interested in the thermal conductivity at room temperature which is lower than the Debye temperature Θ_D of the silicon system (∼640 K), a quantum correction to the MD calculated thermal conductivity should be considered [36, 37]. Our results are carefully tested with respect to the size of the simulation box, and we find that a $10 \times 10 \times 10$ supercell is good enough to yield a converged thermal conductivity. To confirm the reliability of our calculations, the thermal conductivity of bulk Si at 1000 K is calculated, and we find that the value of 62 $\mathrm{W\,m^{-1}\,K^{-1}}$ agrees well with previously reported result [32] of 61 $\mathrm{W\,m^{-1}\,K^{-1}}$.

3 Results and discussions

We begin our investigation with *np*Si. The upper panel of Fig. 2 shows two *np*Si with periodically arranged squared

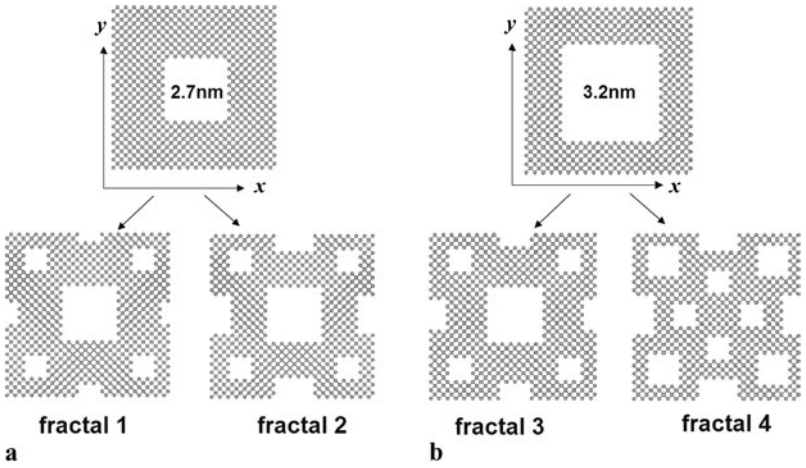

Fig. 2 Top views of nanoporous Si with pore sizes of (**a**) 2.7 nm, and (**b**) 3.2 nm. The corresponding fractal-like patterns are also shown

pores in the (001) plane of bulk Si. The systems are simulated in a $5.4 \times 5.4 \times 5.4$ nm^3 box. In our calculations, different pore sizes (from 2.2 to 3.7 nm) are considered and the corresponding thermal conductivities at 300 K are summarized in Table 1. Compared with that of bulk Si ($\sim$150 W m^{-1} K^{-1} at 300 K), we find that the thermal conductivity of *np*Si is reduced significantly. Moreover, the thermal conductivity decreases monotonically with increasing pore size. For an *np*Si with pore size of 3.7 nm, the calculated conductivity is only 1.3 W m^{-1} K^{-1}, about two orders of magnitude smaller than that of bulk Si. This observation is in reasonable agreement with Lee's results [19] and it is believed that the reduced thermal conductivity comes from the increased phonon scattering by the pore surface. However, large pore size indicates large porosity of the system, which may lead to poor electrical conductivity and is unfavorable for its thermoelectric performance. We thus focus on the *np*Si with relatively smaller pore size, which are 2.7 and 3.2 nm as indicated in Fig. 2. In addition to a single pore in the unit cell, we have introduced many smaller pores which are arranged as a fractal structure. As shown in the lower panel of Fig. 2, these nanostructure-patterned silicon samples have larger surface area and may further decrease the thermal conductivity by increased phonon scattering. Table 2 gives the calculated room temperature thermal conductivity of these patterns labeled as fractal 1, 2, 3, and 4. For comparison, the results of *np*Si with a single pore are also shown. We first focus on the 2.7 nm single pore and its corresponding nanostructure patterns (fractal 1 and fractal 2). We see that although they have almost the same porosity, the fractal-like structures indeed have much smaller thermal conductivities. It is interesting to note that the thermal conductivity decreases monotonically with increased surface area. This is also the case for the 3.2 nm single pore and its corresponding nanostructure patterns. We see that although the four fractal-like patterns have similar porosity, the fractal 4 has the lowest thermal conductivity (0.6 W m^{-1} K^{-1}) which is consistent with its largest surface area. The fractal-like pattern thus provides a very efficient way to reduce the thermal conductivity of *np*Si without increasing the porosity.

Table 1 Calculated room temperature thermal conductivity of nanoporous Si with different pore size

Pore sizes (nm)	2.2	2.7	3.2	3.7
κ (W m^{-1} K^{-1})	11.1	6.6	4.4	1.3

Table 2 Calculated room temperature thermal conductivity of 2.7 and 3.2 nm *np*Si and their fractal-like structures. The corresponding porosity and surface area are also given

Pattern	Porosity (V_{npSi}/V_{bulk})	Surface areas (nm^2)	κ (W m^{-1} K^{-1})
2.7 nm single pore	0.23	59.0	6.6
fractal 1	0.20	147.4	1.9
fractal 2	0.23	159.2	1.0
3.2 nm single pore	0.33	70.8	4.4
fractal 3	0.27	171.0	2.0
fractal 4	0.29	224.1	0.6

We next consider Si nanofilm which may also have small thermal conductivity due to surface scattering of phonons. Compared with the Si NWs, the two-dimensional Si nanofilm can be easily fabricated by many methods such as molecular beam epitaxy or Czochralski process. To calculate the thermal conductivity of two-dimensional silicon, a non-periodic and shrink-wrapped boundary condition is employed in the z-direction and a simulation box with 0.9 nm vacancy layer is used so that the nanofilm can be treated as independent entity. Figure 3(a) shows the Si (001) nanofilm with a section of 3.9×3.9 nm^2 in the xy-plane. We have calculated the room temperature in-plane thermal conductivity with thicknesses of 4.8 and 1.6 nm. We found that the corresponding value is reduced from 48 to 14 W m^{-1} K^{-1}, and

Table 3 Calculated thermal conductivity along x- and y-directions of etched Si nanofilm with different orientations

Orientations	κ_{xx} (W m^{-1} K^{-1})	κ_{yy} (W m^{-1} K^{-1})
(001)	0.8	8.2
(110)	3.5	60
(111)	0.9	4.0

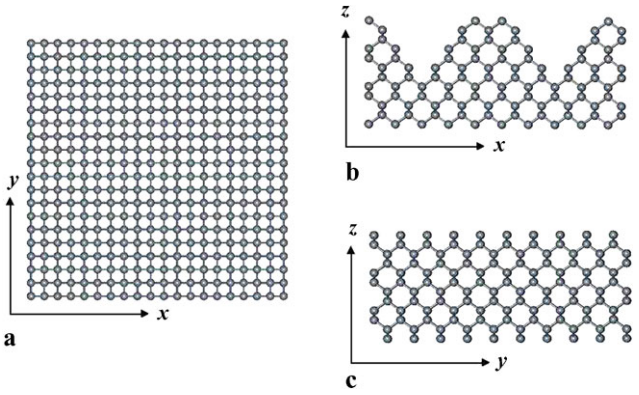

Fig. 3 (**a**) Top view of Si nanofilm, (**b**) side view of etched Si nanofilm from the y-direction, and (**c**) side view of etched Si nanofilm from the x-direction

both are much smaller than that of bulk Si. To get very small thermal conductivity, one should thus make the nanofilm as thin as possible. In addition, surface roughness is introduced into the Si nanofilms to further scatter phonons. Here we consider the Si (001) nanofilm with thickness of 1.6 nm. The roughness can be generated by chemically etched grooves against the x-direction. In the present work, the depth of the grooves is set to ∼0.8 nm and the width is ∼4 nm. It is expected that the rough surface will reduce the thermal conductivity while the underlying prefect Si layers would maintain good electronic transport. Figures 3(b) and 3(c) give side views of such etched Si nanofilm. The corresponding thermal conductivities κ_{xx} and κ_{yy} are calculated and listed in Table 3. For comparison, we have done additional calculations where the thermal conductivities of Si (110) and (111) etched nanofilms are also obtained. We see that the thermal conductivity shows strong anisotropy and κ_{xx} is significantly smaller than κ_{yy}. This is reasonable since the grooves are etched along the y-direction and the surface roughness along the x-direction causes strong phonon scattering. The same thermal conductivity anisotropy can be found for the Si (110) and (111) nanofilms. It is interesting to find that the thermal conductivity along the x-direction shows an orientation dependence, in the order of $\kappa_{xx}(001) < \kappa_{xx}(111) < \kappa_{xx}(110)$. Our theoretical results suggest that in the fabrication of Si nanofilm, it should be (001) oriented in favor of its thermoelectric application.

The third system we consider is a quasi-periodic layered SiGe. In the unit cell of such a system, the Si and Ge (001) layers are arranged according to the Fibonacci number N, which can be expressed as:

Table 4 Calculated thermal conductivity along x-, y-, and z-directions of quasi-periodic layered SiGe structures according to different Fibonacci numbers

Fibonacci number	κ_{xx} (W m^{-1} K^{-1})	κ_{yy} (W m^{-1} K^{-1})	κ_{zz} (W m^{-1} K^{-1})
8	70	105	0.6
13	38	98	2.0
21	60	50	0.3
34	80	95	0.7

1:B; 1:A; 2:AB; 3:ABA; 5:ABAAB; 8:ABAABABA . . .

Here A and B represent one Si (001) or Ge (001) layer, and each is buckled. For a big unit cell corresponding to the Fibonacci number 21, the system can be written as:

. . . |SiGeSiSiGeSiGeSiSiGeSiSiGeSiGeSiSiGeSiGeSi| . . .

Note that if the Fibonacci number is odd, one more Si layer will be added into the unit cell to maintain the periodic boundary condition. Figure 4 is a side view of the unit cell where the Si and Ge (001) layers are arranged according to the Fibonacci number 21. This quasi-periodically patterned unit cell repeats along the z-direction to form a special bulk SiGe. Table 4 summarizes the calculated room temperature thermal conductivity of such a system with different Fibonacci numbers ($N = 8, 13, 21, 34$). For all the systems we considered, we find that the thermal conductivity shows strong anisotropy. The κ_{zz} is significantly smaller than κ_{xx} and κ_{yy}, which can be attributed to the quasi-periodic patterning along the z-direction. The broken periodic boundary condition within the unit cell could effectively increase phonon scattering and thus largely suppress the thermal conductivity. Compared with the fractal and groove patterning discussed above, it seems that quasi-periodic patterning is more efficient to reduce the thermal conductivity. For the system having Fibonacci number 21, the thermal conductivity can be reduced to 0.3 W m^{-1} K^{-1}, which is about 1/500 of that found for bulk Si.

The ultra-small thermal conductivity of the quasi-periodic layered SiGe suggests its favorable thermoelectric properties. As mentioned before, the efficiency of a thermoelectric material is determined by the ZT value which includes both the electron and phonon transport coefficients. The electronic transport can be essentially derived from first-principles calculations. For simplicity, here we consider the quasi-periodic SiGe system having Fibonacci number 8. Our first-principles calculations have been performed using a plane-wave pseudopotential formulation [38–40], as implemented in the Vienna ab initio simulation package

(VASP). We use ultrasoft pseudopotentials for the Si and Ge atoms and a cutoff energy of 150 eV. We adopt a hexagonal supercell with dimension of 3.8 Å × 3.8 Å × 25.5 Å, and the Brillouin zone is sampled with 9 × 9 × 2 Monkhorst–Pack meshes. Optimal atomic positions are determined until the magnitude of the forces acting on all atoms become less than 0.05 eV/Å. The calculated band structure is shown in Fig. 5(a). For comparison, the band structure of bulk Si with eight (001) layers in one unit cell is plotted in Fig. 5(b). We see that although they have different atomic arrangement inside the unit cell, their band structures are almost the same except for slight changes in the conduction bands along the Γ–Z direction. This implies that the electronic transport would not be changed much by quasi-periodic patterning of Si and Ge. It is worth mentioning that the bandgap is reduced from 0.39 to 0.30 eV by quasi-periodic patterning, and the conduction bands along the Γ–Z direction become flatter. All these facts suggest that the quasi-periodic layered SiGe structure will have the same or even better electronic transport properties than that of bulk Si. Considering the fact that the thermal conductivity is reduced by ∼500 times, it is thus reasonable to estimate that the ZT value of the quasi-periodic SiGe system can be enhanced to ∼5.0, which makes it a very appealing thermoelectric material and needs further experimental and theoretical investigations.

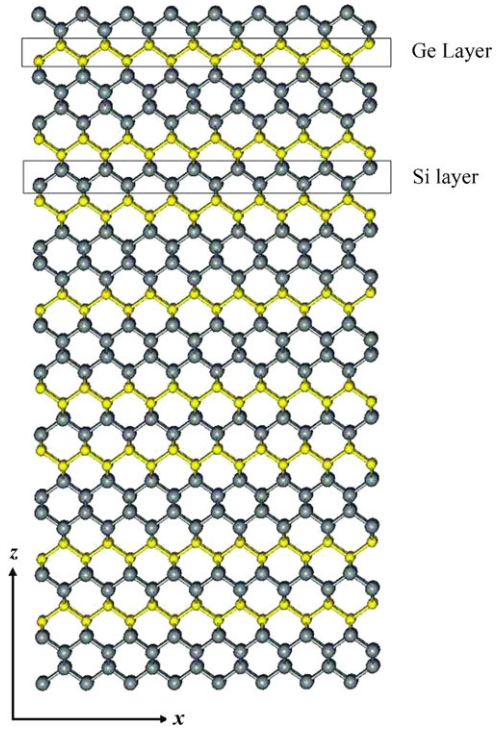

Fig. 4 The unit cell of quasi-periodic layered SiGe structures according to the Fibonacci number 21

4 Summary

In summary, we show by MD simulations that nanoporous Si exhibits a very small thermal conductivity compared with that of bulk Si, and the fractal-like patterning can further reduce it due to increased surface scattering. The thermal conductivity of Si nanofilm decreases when the film becomes thinner, and can be also significantly suppressed by etching nanoscale grooves on its surface. The ultra-small thermal conductivity (0.3 $\mathrm{W\,m^{-1}\,K^{-1}}$) can be achieved when the Si and Ge monolayer are quasi-periodically arranged in the unit cell. Without changing much to the electronic transport of bulk Si, the nanostructure-patterned Si materials could have very promising thermoelectric applications.

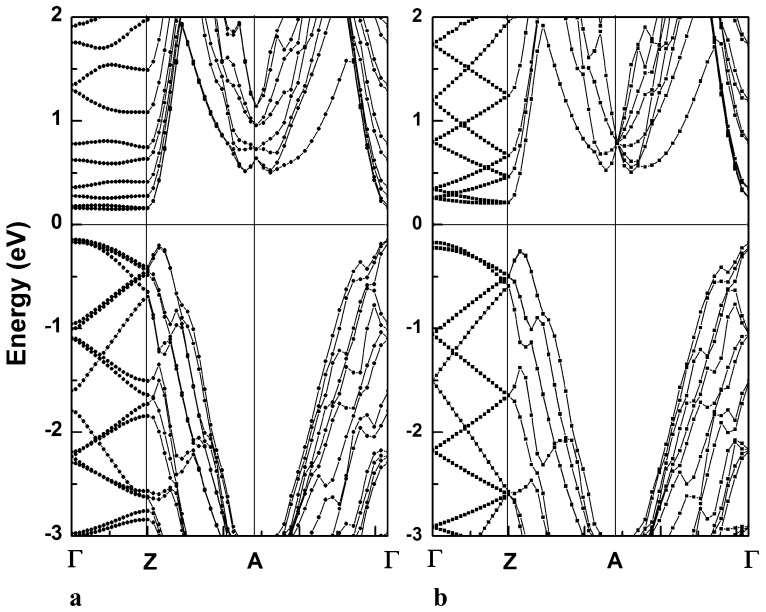

Fig. 5 Calculated band structures of (**a**) quasi-periodic layered SiGe structure having Fibonacci number 8, and (**b**) bulk Si with eight (001) layers in one unit cell

Acknowledgements This work was supported by the "973 Program" of China (Grant No. 2007CB607501), the National Natural Science Foundation (Grant No. 51172167), and the Program for New Century Excellent Talents in University. We also acknowledge financial support from the interdiscipline and postgraduate programs under the "Fundamental Research Funds for the Central Universities". All the calculations were performed in the PC Cluster from Sugon Company of China.

References

1. L.D. Hicks, M.S. Dresselhaus, Phys. Rev. B **47**, 12727 (1993)
2. L.D. Hicks, M.S. Dresselhaus, Phys. Rev. B **47**, 16631 (1993)
3. D.M. Rowe, V.S. Shukla, N. Savvides, Nature **290**, 765 (1981)
4. G. Joshi, H. Lee, Y.C. Lan, X.W. Wang, G.H. Zhu, D.Z. Wang, R.W. Gould, D.C. Cuff, M.Y. Tang, M.S. Dresselhaus, G. Chen, Z.F. Ren, Nano Lett. **8**, 4670 (2008)
5. X.W. Wang, H. Lee, Y.C. Lan, G.H. Zhu, G. Joshi, D.Z. Wang, J. Yang, A.J. Muto, M.Y. Tang, J. Klatsky, S. Song, M.S. Dresselhaus, G. Chen, Z.F. Ren, Appl. Phys. Lett. **93**, 193121 (2008)
6. G.H. Zhu, H. Lee, Y.C. Lan, X.W. Wang, G. Joshi, D.Z. Wang, J. Yang, D. Vashaee, H. Guilbert, A. Pillitteri, M.S. Dresselhaus, G. Chen, Z.F. Ren, Phys. Rev. Lett. **102**, 196803 (2009)
7. S.-M. Lee, D.G. Cahill, R. Venkatasubramanian, Appl. Phys. Lett. **70**, 2957 (1997)
8. S.T. Huxtable, A.R. Abramson, C.-L. Tien, A. Majumdar, C. LaBounty, X. Fan, G. Zeng, J.E. Bowers, A. Shakouri, E.T. Croke, Appl. Phys. Lett. **80**, 1737 (2002)
9. V. Samvedi, V. Tomar, J. Appl. Phys. **105**, 013541 (2009)
10. V. Samvedi, V. Tomar, Nanotechnology **20**, 365701 (2009)
11. D. Li, Y. Wu, P. Kim, L. Shi, P. Yang, A. Majumdar, Appl. Phys. Lett. **83**, 2934 (2003)
12. I. Ponomareva, D. Srivastava, M. Menon, Nano Lett. **7**, 1155 (2007)
13. A.I. Hochbaum, R. Chen, R.D. Delgado, W. Liang, E.C. Garnett, M. Najarian, A. Majumdar, P. Yang, Nature **451**, 163 (2008)
14. A.I. Boukai, Y. Bunimovich, J. Tahir-Kheli, J. Yu, W.A. Goddard, J.R. Heath, Nature **451**, 168 (2008)
15. N. Mingo, L. Yang, D. Li, A. Majumdar, Nano Lett. **3**, 1713 (2003)
16. N. Mingo, D.A. Broido, Phys. Rev. Lett. **93**, 246106 (2004)
17. D. Donadio, G. Galli, Phys. Rev. Lett. **102**, 195901 (2009)
18. J. Chen, G. Zhang, B. Li, Appl. Phys. Lett. **95**, 073117 (2009)
19. J-H. Lee, J.C. Grossman, J. Reed, G. Galli, Appl. Phys. Lett. **91**, 223110 (2007)
20. C. Bera, N. Mingo, S. Volz, Phys. Rev. Lett. **104**, 115502 (2010)
21. J. Tang, H. Wang, D.H. Lee, M. Fardy, Z. Huo, T.P. Russell, P. Yang, Nano Lett. **10**, 4279 (2010)
22. P.E. Hopkins, C.M. Reinke, M.F. Su, R.H. Olsson III, E.A. Shaner, Z.C. Leseman, J.R. Serrano, L.M. Phinney, I. El-Kady, Nano Lett. **11**, 107 (2011)
23. J.-H. Lee, G.A. Galli, J.C. Grossman, Nano Lett. **8**, 3750 (2008)
24. S. Plimpton, J. Comput. Phys. **117**, 1 (1995). Code available at: http://lammps.sandia.gov/download.html
25. W.G. Hoover, D.J. Evans, R.B. Hickman, A.J.C. Ladd, W.T. Ashurst, B. Moran, Phys. Rev. B **22**, 1690 (1980)
26. W.G. Hoover, A.J.C. Ladd, B. Moran, Phys. Rev. Lett. **48**, 1818 (1982)
27. D. MacGowan, D.J. Evans, Phys. Rev. A **34**, 2133 (1986)
28. D. MacGowan, D.J. Evans, Phys. Rev. A **36**, 948 (1987)
29. G.V. Paolini, G. Ciccotti, Phys. Rev. A **35**, 5156 (1987)
30. P. Sindzingre, G. Ciccotti, C. Massobrio, D. Frenkel, Chem. Phys. Lett. **136**, 35 (1987)
31. R. Vogelsang, C. Hoheisel, G. Paolini, G. Ciccotti, Phys. Rev. A **36**, 3964 (1987)
32. P.K. Schelling, S.R. Phillpot, P. Keblinski, Phys. Rev. B **65**, 144306 (2002)
33. F.H. Stillinger, T.A. Weber, Phys. Rev. B **31**, 5262 (1985)
34. J. Tersoff, Phys. Rev. B **39**, 5566 (1989)
35. T. Markussen, A.P. Jauho, M. Brandbyge, Nano Lett. **8**, 3771 (2008)
36. Q.H. Tang, Mol. Phys. **102**, 1959 (2004)
37. L. Sun, J.Y. Murthy, Appl. Phys. Lett. **89**, 171919 (2006)
38. G. Kresse, J. Hafner, Phys. Rev. B **47**, 558 (1993)
39. G. Kresse, J. Hafner, Phys. Rev. B **49**, 14251 (1994)
40. G. Kresse, J. Furthmüller, Comput. Mater. Sci. **6**, 15 (1996)